IEEE PEDS 2017, Honolulu, USA
12 - 15 December 2017

A Unified SVPWM Realization for Minimizing Circulating Currents of Dual Three Phase Machines

Hisham Eldeeb, Christoph Hackl
Munich School of Engineering
Technical University of Munich (TUM)
Munich, Germany
E-mail: hisham.eldeeb@tum.de

Mohamed Abdelrahem
Institute of Electrical Drives systems and Power Electronics, TUM
Munich, Germany

Ayman Samy Abdel-Khalik
Electrical Engineering Department
Faculty of Engineering, Alexandria University
Alexandria, Egypt.

***Abstract*—Space-vector PWM (SVPWM) gained attention, as a voltage synthesis technique for asymmetrical dual three phase machines (ADTMs); due to its ability to minimize the harmonic content of the output and minimize the switching losses through proper selection of the switching vectors. It has been studied extensively for ADTMs mainly for induction machines with isolated neutrals (2N), such that the inverter is assumed to be the only source capable of inducing harmonics within the stator currents. Thus, by setting the xy subspace voltages to zero, the harmonic content is minimized. However, for dual three phase-permanent magnet synchronous machines (DT-PMSM), the presence of non-sinusoidal rotor flux invokes significant harmonics, mandating non-zero references for the xy plane to ensure proper compensation. This paper invokes the employment of non-zero harmonic references within the SVPWM calculation for the 2N connection, as well as laying out the fundamentals for the single neutral (1N) connection, which is more reliable from fault-tolerance point of view. Also, a simple digital realization is presented, suitable for the 12-, 24-sector SVPWM methods, both continuous and discontinuous modulations. The theoretical findings are corroborated with a 4.4 kW DT-PMSM, demonstrating significant improvement in the total harmonic distortion (THD) of the stator currents.**

***Index Terms*—Dual three phase IPMSM, dual three phase inverter, SVPWM.**

NOMENCLATURE

$\mathbb{R}, \mathbb{N}$ is the set of real and natural numbers. $x \in \mathbb{R}$ is a real scaler, while $\boldsymbol{x} \in \mathbb{R}^n$ (bold) is real valued vector with $n \in \mathbb{N}$. $\boldsymbol{x}^\top$ is the transpose of $\boldsymbol{x}$. $\boldsymbol{X} \in \mathbb{R}^{n\times m}$ (capital bold) is a real valued matrix with $n \in \mathbb{N}$ rows and $m \in \mathbb{N}$ columns. $\boldsymbol{I}_n \in \mathbb{R}^{n\times n} := \mathrm{diag}(1,\ldots,1)$: identity matrix, while $\boldsymbol{O}_n \in \mathbb{R}^{n\times n} := \mathrm{diag}(0,\ldots,0)$: zero square matrix. $\boldsymbol{x}_{\mathrm{s}}^{a_1\to c_2} \in \mathbb{R}^n$ is the stator space vector expressed in the natural *($\mathrm{a_1b_1c_1}$-$\mathrm{a_2b_2c_2}$)* reference frame and may represent voltage $\boldsymbol{u}$ (in V), flux linkage $\boldsymbol{\psi}$ (in Wb) or current $\boldsymbol{i}$ (in A), i.e. $\boldsymbol{x} \in \{\boldsymbol{u}, \boldsymbol{\psi}, \boldsymbol{i}\}$. The subscript 's' donates referencing to the stator. The electromechanical and load torques (in Nm), the rotor electrical angular speed (in rad/s), electrical angular position (in rad) with respect to the reference flux axis of phase *a*, and inertia (in kgm^2) are represented by m_{m}, m_{load}, ω_{k}, ϕ_{k}, and Θ, respectively. The viscous friction is represented by ν (in $\mathrm{N\,m\,s^{-1}}$). The electrical resistance (in Ω) and inductances (in H) are indicated by R and L, respectively.

I. INTRODUCTION

The last decade experienced an increasing interest in multi-phase machines in general; owing to their inherent fault-tolerance capability, enhanced efficiency, rating reduction of the employed voltage source inverter (VSI), and lower torque ripples compared to conventional three phase machines [1]–[7]. Dual three phase machines (DTM) are of particular interest, since the windings of conventional three phase machines could be replaced without, dramatic changes, by six phase windings. The employment of DTMs is addressed from three main aspects: machine design [3], [4], neutral points connection [5], and proper syntheses of the demanded reference voltage [4], [6]–[8]. Asymmetrical DTM (ADTM) (i.e. spatial phase shift of $\pi/6$ rad between the two three phase sets $a_1b_1c_1$-$a_2b_2c_2$) intrinsically attain the ability to provide an improved harmonic content of flux linkage, thus enhanced efficiency and lower space harmonics. When combining such machine with a space-vector pulse-width-modulation-based (SVPWM) VSI, switching losses and switches commutations are minimized, along with enhanced stator current quality. Upon applying the vector space decomposition technique [7]–[9], the choice of the variously discussed SVPWM schemes is dependant on: (i) spatial phase shift between the two three phase sets (in this paper $\pi/6$ rad), (ii) the effect of the chosen switching vectors on exciting (xy) harmonics and zero-sequence (0^+0^-) currents, and (iii) challenges concerning practical digital implementation of the chosen SVPWM scheme. It was pointed out in [9] that the impedance of the equivalent circuit in the xy and 0^+0^- plane of a practical DTM could be a few percentage of the fundamental impedance. Therefore, a minor degree of unbalance of the supplied stator voltages, at such low harmonic impedances, could easily excite the harmonic planes with significant currents that would only contribute to the stator ohmic losses and the VSI semiconductor losses. Achieving minimum currents in both xy and 0^+0^- planes is attested by minimizing per switching period the distance between the resultant voltages in xy and 0^+0^- planes and the origin (i.e. minimising those currents from control point of view); and/or maximizing their equivalent impedance (i.e. machine design point of view), where the former is the main topic in this paper. Isolating the two neutral points (2N) of the dual three phase

978-1-5090-2364-6/17$31.00

sets has the consequence of completely eliminating the zero-sequence currents and higher utilization of the available DC-link voltage. Accordingly, the 2N configuration was endorsed in several publications [6]–[8], especially for DT-induction machines (DT-IM), showing several SVPWM manipulations and the corresponding effect on the stator current harmonic content, fundamental component, and switching losses. For DT-permanent magnet synchronous machines (DT-PMSM), the non-ideal non-sinusoidal rotor flux would result in a non-sinusoidal back-electromotive force (*emf*), which would contribute, beside the DT-inverters, to the harmonic currents. Thus, setting the reference voltages to zero in the harmonic planes would only compensate for the inverter harmonics, leading to distorted stator currents with significant torque ripples [10].

In terms of practical realization, although the 12-sector SVPWM method requires less memory than the 24-sector method to store the offline precomputed dwell times per sectors, it faces challenges to implement digitally and may require an additional hardware board to assist in successful implementation [6]. Moreover, the total number of transitions (i.e switching from ON $\leftrightarrow$ OFF) is considerably high to synthesize the desired reference voltage. Thus, the 24-sector PWM technique was introduced in [7], [8], [11], simplifying the digital implementation and reducing the harmonic content.

This paper illustrates the necessity to account for non-zero harmonic references and encompass them within the precomputed dwell timings for the 12-, 24-sector SVPWM techniques utilized for 2N configuration; making it suitable for DT-PMSMs. Also, a simple digital implementation strategy is presented, which is suitable for the aforementioned SVPWM techniques (i.e. 12-, 24-sector and the modified 24-sector methods) and accommodates both continuous and discontinuous SVPWM methods. This strategy could also be used as a *plug-in* that can be extended to include the implementation of SVPWM strategies within the over-modulation region [12]. In addition to this, the fundamentals for an adequate SVPWM for a 1N connection will be demonstrated, since the 1N connection is characterized by better fault-tolerance capability [5]. The presented theoretical findings are experimentally tested on a 4.4 kW ADT-interior PMSM (ADT-IPMSM).

II. Asymmetrical dual three phase drive model

A. Dual three phase IPMSM Model

Motivated by the simplicity of modelling and controlling of early DC machines, where stationary orthogonal armature (i.e. stator) flux and field flux existed, the Clarke transformation was introduced for three-phase drives, decomposing the $2\pi/3$ spatially distributed three-phase fluxes into two-orthogonal $\alpha\beta$ flux axes in the same subspace (i.e. electromechanical energy conversion subspace), and one remaining axis orthogonal to the $\alpha\beta$ subspace, which is also known as the *zero* "0" subspace. Upon applying the rotating Park transformation, the machine model attain similarities with earlier DC machines, where the *d*-axis component is directly correlated with the flux within the air-gap and the orthogonal *q*-axis component controls the generated electromechanical torque m_{m}. With the development of electrical machines, as in this case IPMSM, as well as the different optimisation techniques, both the $dq-$ fluxes are optimised for a given m_{m} to minimise the stator-coper losses [13].

Similarly, for a DTM drive, a generalised Clarke transformation, also known as vector space decomposition (VSD),

$$\boldsymbol{T}_{\mathrm{VSD}} = \frac{1}{3}\begin{bmatrix} 1 & -\frac{1}{2} & -\frac{1}{2} & \frac{\sqrt{3}}{2} & -\frac{\sqrt{3}}{2} & 0 \\ 0 & \frac{\sqrt{3}}{2} & -\frac{\sqrt{3}}{2} & \frac{1}{2} & \frac{1}{2} & -1 \\ 1 & -\frac{1}{2} & -\frac{1}{2} & -\frac{\sqrt{3}}{2} & \frac{\sqrt{3}}{2} & 0 \\ 0 & -\frac{\sqrt{3}}{2} & \frac{\sqrt{3}}{2} & \frac{1}{2} & \frac{1}{2} & -1 \\ 1 & 1 & 1 & 0 & 0 & 0 \\ 0 & 0 & 0 & 1 & 1 & 1 \end{bmatrix}, \quad (1)$$

mapping the six-phases to three orthogonal planes, namely the equivalent $\alpha\beta$ subspace, 0^+0^- in the "0" subspace representing the *zero* sequence components from both three-phase sets, and the xy subspace, which directly controls the degree of unbalance between the three-phase sets and derating factors during faults [1], [2], [5]. Using the generalised Park transformation [14]

$$\overline{\boldsymbol{T}}_p(\phi_{\mathrm{k}})^{-1} = \begin{bmatrix} \boldsymbol{T}_{\mathrm{p}}(\phi_{\mathrm{k}})^{-1} & \boldsymbol{O}_2 & \boldsymbol{O}_2 \\ \boldsymbol{O}_2 & \boldsymbol{T}_{\mathrm{p}}(-\phi_{\mathrm{k}})^{-1} & \boldsymbol{O}_2 \\ \boldsymbol{O}_2 & \boldsymbol{O}_2 & \boldsymbol{I}_2 \end{bmatrix}, \quad (2)$$

where $\boldsymbol{T}_{\mathrm{p}}(\phi_{\mathrm{k}})^{-1} = \begin{bmatrix} \cos(\phi_{\mathrm{k}}) & -\sin(\phi_{\mathrm{k}}) \\ \sin(\phi_{\mathrm{k}}) & \cos(\phi_{\mathrm{k}}) \end{bmatrix}$, the ADTM-IPMSM dynamic model, neglecting saturation, is

$$\left.\begin{aligned} \boldsymbol{u}_{\mathrm{s}}^{k} &= R_{\mathrm{s}}\,\boldsymbol{i}_{\mathrm{s}}^{k} + \omega_{\mathrm{k}}\,\boldsymbol{J}\boldsymbol{\psi}_{\mathrm{s}}^{k} + \tfrac{\mathrm{d}}{\mathrm{d}t}\boldsymbol{\psi}_{\mathrm{s}}^{k}, \\ \boldsymbol{u}_{\mathrm{s}}^{xy} &= R_{\mathrm{s}}\,\boldsymbol{i}_{\mathrm{s}}^{xy} - \omega_{\mathrm{k}}\,\boldsymbol{J}\boldsymbol{\psi}_{\mathrm{s}}^{xy} + \tfrac{\mathrm{d}}{\mathrm{d}t}\boldsymbol{\psi}_{\mathrm{s}}^{xy}, \\ \boldsymbol{u}_{\mathrm{s}}^{0} &= R_{\mathrm{s}}\,\boldsymbol{i}_{\mathrm{s}}^{0} + \tfrac{\mathrm{d}}{\mathrm{d}t}\boldsymbol{\psi}_{\mathrm{s}}^{0}, \\ \tfrac{\Theta}{n_{\mathrm{p}}}\tfrac{\mathrm{d}\omega_{\mathrm{k}}}{\mathrm{d}t} &= \underbrace{3\,n_{\mathrm{p}}\boldsymbol{i}_{\mathrm{s}}^{k\top}\boldsymbol{J}\,\boldsymbol{\psi}_{\mathrm{s}}^{k}}_{:=m_{\mathrm{m}}} - (m_{\mathrm{load}} + \tfrac{\nu}{n_{\mathrm{p}}}\omega_{\mathrm{k}}), \end{aligned}\right\} \quad (3)$$

where $\boldsymbol{J} := \boldsymbol{T}_{\mathrm{p}}(\pi/2)^{-1}$, $\boldsymbol{\psi}_{\mathrm{s}}^{k} = \boldsymbol{L}_{\mathrm{s}}^{k}\,\boldsymbol{i}_{\mathrm{s}}^{k} + \boldsymbol{\psi}_{\mathrm{pm}}^{k}$, $\boldsymbol{L}_{\mathrm{s}}^{k} = \begin{bmatrix} L_l+L_{\mathrm{s}}^{d} & 0 \\ 0 & L_l+L_{\mathrm{s}}^{q} \end{bmatrix}$, $\boldsymbol{i}_{\mathrm{s}}^{k} = \begin{pmatrix} i_{\mathrm{s}}^{d}, & i_{\mathrm{s}}^{q} \end{pmatrix}^{\top}$, the leakage and *dq*-axes inductances are denoted by L_l, L_{s}^{d}, and L_{s}^{q}, respectively, $\boldsymbol{\psi}_{\mathrm{pm}}^{k} = \begin{pmatrix} \psi_{\mathrm{pm}}, & 0 \end{pmatrix}^{\top}$, $\boldsymbol{\psi}_{\mathrm{s}}^{xy} = L_l\,\boldsymbol{i}_{\mathrm{s}}^{xy}$, $\boldsymbol{i}_{\mathrm{s}}^{xy} = \begin{pmatrix} i_{\mathrm{s}}^{x}, & i_{\mathrm{s}}^{y} \end{pmatrix}^{\top}$, $\boldsymbol{\psi}_{\mathrm{s}}^{0} = L_l\,\boldsymbol{i}_{\mathrm{s}}^{0}$, $\boldsymbol{i}_{\mathrm{s}}^{0} = \begin{pmatrix} i_{\mathrm{s}}^{0^+}, & i_{\mathrm{s}}^{0^-} \end{pmatrix}^{\top}$.

B. Dual three-phase Inverter Model

1) 1N/2N inverter model and voltage limits: Dis-, connecting the star points (i.e. 2N and 1N modes) through the designated switch in Fig. 1 is crucial; since it defines the degrees of freedom (i.e. number of independent currents to be controlled), which are *four* for the 2N configuration and *five* for the 1N connection. Assuming balanced phase voltages, the VSI phase voltages $\boldsymbol{u}_{\mathrm{s}}^{\mathrm{ph}} := \begin{pmatrix} u_{\mathrm{s}}^{\mathrm{a}_1}, & u_{\mathrm{s}}^{\mathrm{b}_1}, & u_{\mathrm{s}}^{\mathrm{c}_1}, & u_{\mathrm{s}}^{\mathrm{a}_2}, & u_{\mathrm{s}}^{\mathrm{b}_2}, & u_{\mathrm{s}}^{\mathrm{c}_2} \end{pmatrix}^{\top}$ can

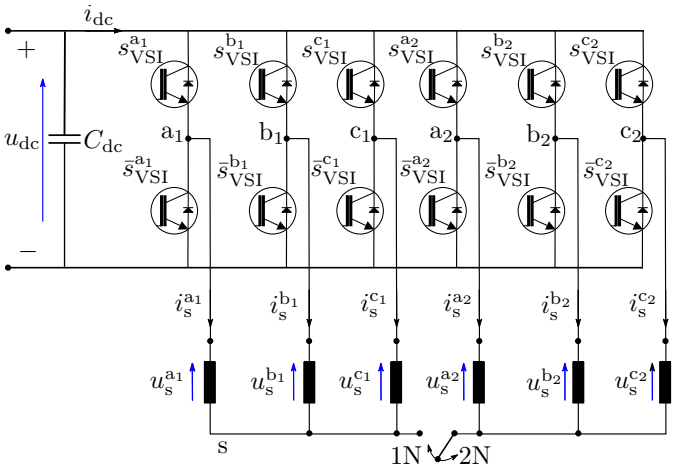

Figure 1: *ADT drive showing the possible 1N/2N connections.*

be expressed for 2N as [8]

$$\boldsymbol{u}^{\mathrm{ph}}_{\mathrm{s}} = \frac{u_{\mathrm{dc}}}{3}\begin{bmatrix} 2 & -1 & -1 & 0 & 0 & 0 \\ -1 & 2 & -1 & 0 & 0 & 0 \\ -1 & -1 & 2 & 0 & 0 & 0 \\ 0 & 0 & 0 & 2 & -1 & -1 \\ 0 & 0 & 0 & -1 & 2 & -1 \\ 0 & 0 & 0 & -1 & -1 & 2 \end{bmatrix} \boldsymbol{s}_{\mathrm{VSI}}, \quad (4)$$

and for 1N [15]

$$\boldsymbol{u}^{\mathrm{ph}}_{\mathrm{s}} = \frac{u_{\mathrm{dc}}}{6}\begin{bmatrix} 5 & -1 & -1 & -1 & -1 & -1 \\ -1 & 5 & -1 & -1 & -1 & -1 \\ -1 & -1 & 5 & -1 & -1 & -1 \\ -1 & -1 & -1 & 5 & -1 & -1 \\ -1 & -1 & -1 & -1 & 5 & -1 \\ -1 & -1 & -1 & -1 & -1 & 5 \end{bmatrix} \boldsymbol{s}_{\mathrm{VSI}}, \quad (5)$$

where $\boldsymbol{s}_{\mathrm{VSI}} := \left(s^{a_1}_{\mathrm{VSI}},\ s^{b_1}_{\mathrm{VSI}},\ s^{c_1}_{\mathrm{VSI}},\ s^{a_2}_{\mathrm{VSI}},\ s^{b_2}_{\mathrm{VSI}},\ s^{c_2}_{\mathrm{VSI}}\right)^{\top}$ is the switching vector, where each of its element represent the switching state per phase $s^{\kappa}_{\mathrm{VSI}} \in \{0, 1\}$ and $\kappa \in \{a_1, b_1, ..., c_2, \}$, where the values 0 and 1 indicate that the upper switch is turned OFF or ON, respectively, while the opposite applies to the lower switch.

2) Space Vector representation: The inverter in Fig. 1 has 64 possible switching states, which can be represented in a binary form $000000 \rightarrow 111111$ (i.e. in decimal form $0 \rightarrow 63$) where the most significant bit corresponds to $s^{c_2}_{\mathrm{VSI}}$ and the least one for $s^{a_1}_{\mathrm{VSI}}$ (in consistency with [6]–[8]). Each state can be mapped to the $\alpha\beta$, xy, and 0^+0^- subspaces with different magnitude and orientation, obtained for 2N and 1N cases by multiplying equations (4) and (5) with $\boldsymbol{T}_{\mathrm{VSD}}$; leading to the space vectors indicated in Figs. 2 (a), (b) and (c), respectively. Note that for the 2N case, the path for the zero sequence currents is blocked and all switching vectors at that case in 0^+0^- subspace are inhibited to the origin. It is observed in Fig. 2(a) that the voltage vectors with highest amplitudes in — correspond to the the minimum voltage vectors in the xy subspace, while the minimum voltage magnitudes in the $\alpha\beta$ subspace correspond to the highest ones in the xy subspace, thus inducing the most significant $\boldsymbol{i}^{xy}_{\mathrm{s}}$. Accordingly, the minimum voltage magnitudes in the $\alpha\beta$ plane are excluded from the selected voltage vectors when carrying out the SVPWM.

III. SVPWM AND CIRCULATING CURRENT MINIMIZATION

In literature, there are two classification of SVPWM applied for DTM with such type of inverters: 12 sector and 24-sector. Each can operate in either the continuous mode (CSVPWM) (see Figs. 3(a)-i, iii), where all inverter switches are toggled per switching period or the discontinuous mode (DSVPWM), where at least one switch is clamped to the *positive* or *negative* DC-link terminals per switching period T_{sw}) as shown in Fig. 3(a)-ii. The former mode is known for its simplicity, but higher switching losses compared to the latter, which achieves better harmonic performance [6]–[8]. For a 2N configuration, four distinct dwell times for the active vectors $t_{V_1} \rightarrow t_{V_4}$ and $t_{V_0} = T_s - \sum_{n=1}^{4} t_{V_n}$ for the zero vector, corresponding to the equivalent volt-second covered by the references $\boldsymbol{u}^{\alpha\beta}_{\mathrm{s,ref}}$ and $\boldsymbol{u}^{xy}_{\mathrm{s,ref}}$ at the sampling instant $T_s = T_{sw}/2$. The dwell times are computed for the 12-, 24-sector methods by [6]–[8]

$$\begin{pmatrix} t_{V_1} \\ t_{V_2} \\ t_{V_3} \\ t_{V_4} \end{pmatrix} = \begin{bmatrix} u^{\alpha}_{\mathrm{s},1} & u^{\alpha}_{\mathrm{s},2} & u^{\alpha}_{\mathrm{s},3} & u^{\alpha}_{\mathrm{s},4} \\ u^{\beta}_{\mathrm{s},1} & u^{\beta}_{\mathrm{s},2} & u^{\beta}_{\mathrm{s},3} & u^{\beta}_{\mathrm{s},4} \\ u^{x}_{\mathrm{s},1} & u^{x}_{\mathrm{s},2} & u^{x}_{\mathrm{s},3} & u^{x}_{\mathrm{s},4} \\ u^{y}_{\mathrm{s},1} & u^{y}_{\mathrm{s},2} & u^{y}_{\mathrm{s},3} & u^{y}_{\mathrm{s},4} \end{bmatrix}^{-1} \begin{pmatrix} u^{\alpha}_{\mathrm{s,ref}} \\ u^{\beta}_{\mathrm{s,ref}} \\ u^{x}_{\mathrm{s,ref}} \\ u^{y}_{\mathrm{s,ref}} \end{pmatrix} T_s, \quad (6)$$

where each of the column elements of the inverse matrix is the result of substituting the selected active voltage vectors in (4), with the exception that $\boldsymbol{u}^{xy}_{\mathrm{s,ref}} \neq 0$. For instance, assuming the reference $\boldsymbol{u}^{\alpha\beta}_{\mathrm{s,ref}}$ is as shown in Fig. 2(a), the possible vectors for the CSVPWM24 as in [7] within sector I are 40, 41, 9, 11, 15, where t_{V_1} is divided equally among vectors 40 and 15 (see Fig. 3(a)-i) [7]. Since the ADT-voltage dodecagon is symmetric, a number of unique dwell times can be computed offline, stored on the real-time DSP; reducing the execution time of the SVPWM. For instance, it is required to store 6 dwell times for the 12-sector method [6], 12 dwell times for the 24-method [8], and 32 for the modified 24-sector method in [7], which is the 24-sector method adopted in this paper. However, since $\boldsymbol{u}^{xy}_{\mathrm{s,ref}} \neq 0$ and by excerpting the selected switching vectors in [6]–[8], the memory requirements of the real-time platform to store the offline-precomputed dwell times would double, to account for $\boldsymbol{u}^{xy}_{\mathrm{s,ref}}$.

On the other hand, for a 1N configuration, the triplets harmonics are no longer restrained to zero. Within the 0^+0^- subspace, $i^{0^+}_{\mathrm{s}} = -i^{0^-}_{\mathrm{s}}$, which is observable in Fig. 2(c). The additional degree of freedom adds an additional degree dwell time t_{V_5}. It is worth to mention that for the 1N connection the zero vectors for SVPWM are reduced to only two vectors 0 and 63, excluding the vectors 56 and 7 which have highest magnitudes in the 0^+0^- subspace as highlighted with — in Fig. 2(c). Since the aim is to minimize harmonic currents excitation, either 56 and 7 would be excluded from the possible voltage vectors (i.e. similar to neglecting vectors

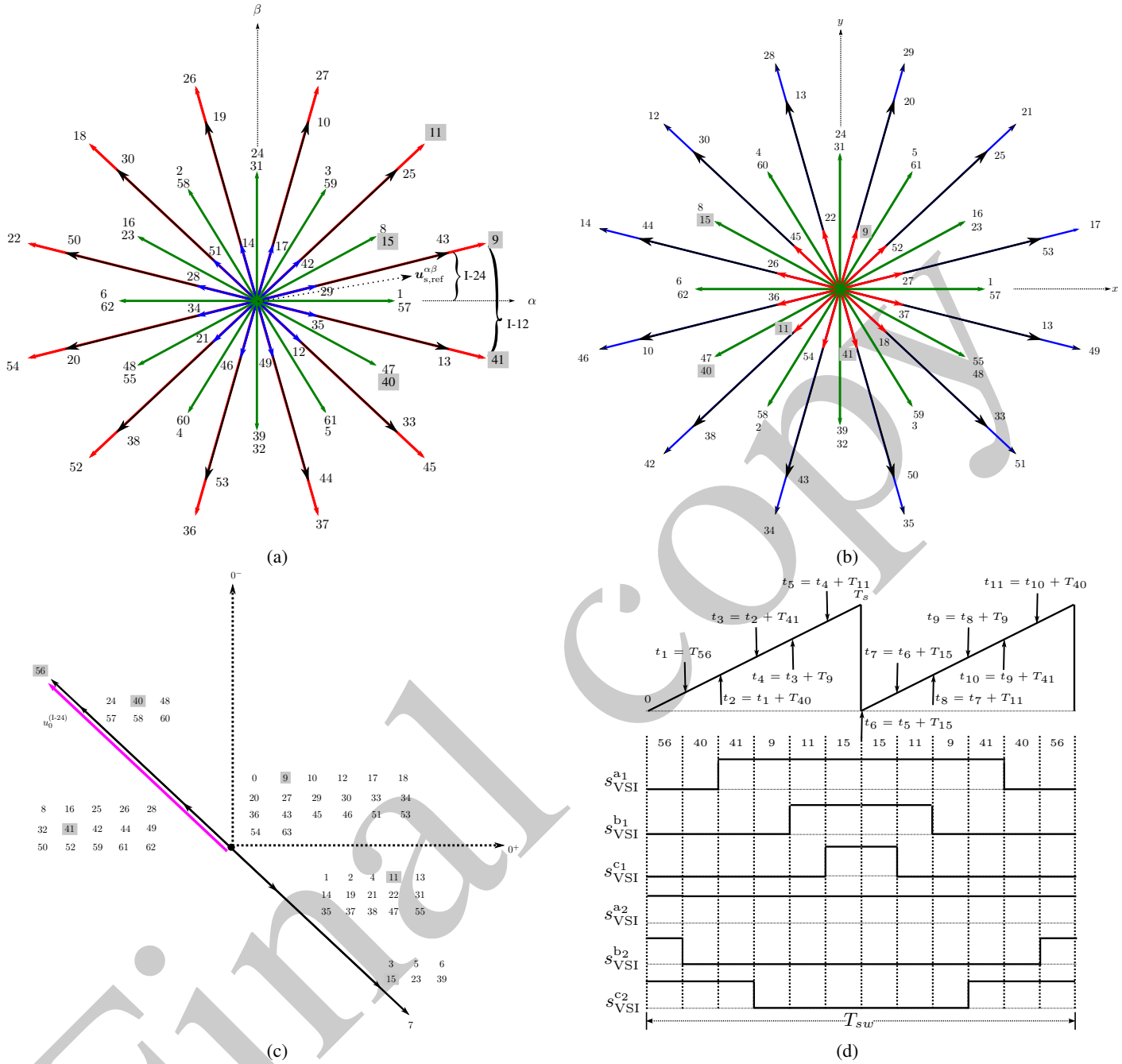

Figure 2: *Voltage space vectors in the (a) fundamental $\alpha\beta$ plane with reference voltage $u_{\alpha\beta}^{ref}$, (b) harmonic xy plane (voltage vectors (0, 7, 56, 63) at their origins, (c) 0^+0^- plane showing residual voltage $u_0^{(I-24)}$ for sector I-24 per T_s and (d) the corresponding timing diagram.*

highlighted in — for the 2N case) or use both per half-cycle as in the CSVPWM24 case (vectors 40 and 15), where the computed t_{V_5} would be distributed evenly among them; leading to average zero voltage per T_{sw}. For instance for the same switching sequence used for sector I in DSVPWM24 upon adding the proper zero vectors, the switching sequence would be (0-56-40-41-9-11-15-7-0 | 0-7-15-11-9-41-40-56-0). It is also worth to mention, that due to the reduced number of zero vectors to only 0 and 63, the DSVPWM would not exist in the 1N mode, leading to higher switching losses compared to the 2N case. At the moment, different tests and switching sequences are investigated and will be reported soon in the near future.

IV. Digital SVPWM Implementation

An important aspect for any PWM technique is the degree of complexity involved for digital realization. One of the main motivations for adopting the 24-sector SVPWM method, compared to 12-sector SVPWM, was the easiness of converting the computed timings into duty cycles (ratio between ON time and switching period T_{sw}) passed to six timers, each responsible

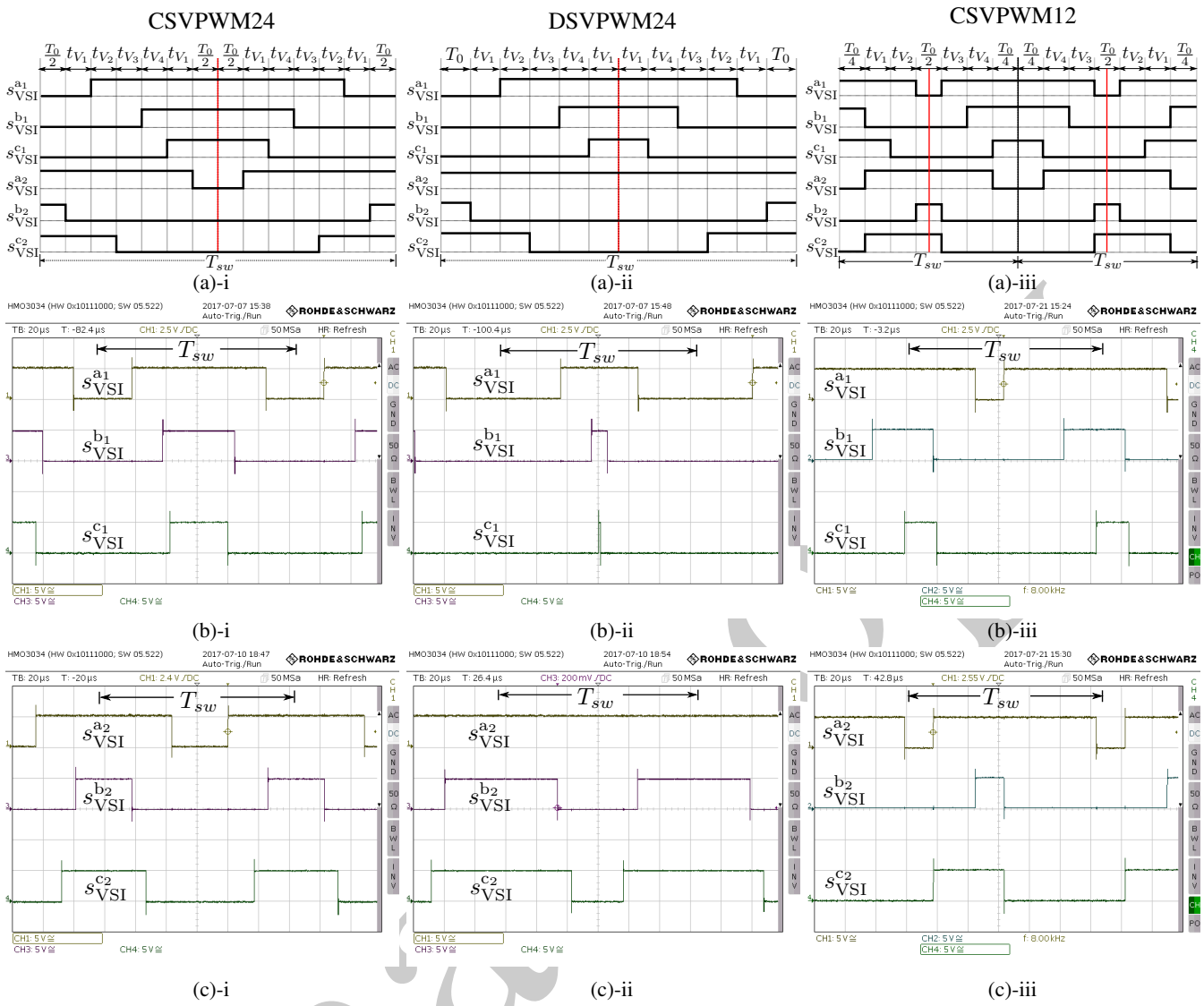

Figure 3: *(a) Simulation and (b)-(c) experimental switching patterns for CSVPWM24, DSVPWM24, and CSVPWM12 for* $\boldsymbol{u}_{\mathrm{s,ref}}^{\alpha\beta}$ *in Fig. 2(a).*

for modulating the voltage per inverter leg [8]. In [7], the developed method enables the decoupling of the six phase VSI into two three phase VSIs modulated with two decoupled three-phase SVPWM. For instance, the switching states in sector I for the 24-sector method (labeled I-24 in Fig. 2(a)) in the continuous mode is (56-40-41-9-11-15-7|7-15-11-9-41-40-56), with the corresponding timing diagram in Fig. 2(d). It clear that each three-phase set start the switching period with the same high/low logic per set, which is the case for any other sector or SVPWM method. Upon identifying the starting logic, and plotting the timing diagram for the remaining sectors, the duty cycles per phase can be computed per sector by observing its relation with the switching states timings. For instance, the ON time for phase a is $2\,(T_{41}+T_9+T_{11}+T_{15})$, while for phase u is $2\,T_{56}$. Alternatively, in this paper a simple proposed method is capable of realizing both methods and also suitable for available DSPs, which developed rapidly throughout the last decade. By identifying the starting logic per set per sector, the ON and OFF times, each leg state can be toggled upon completing the ON/OFF times. For instance, for sector I-24 in Fig. 2(a)), $s_{\mathrm{VSI}}^{\mathrm{a_1}}$ starts with a "0" logic, toggled to "1" after $T_{56}+T_{40}$ (half the OFF time), and switched back to zero upon completing the ON time. By assigning the respective timings per switching states per sector (i.e. T_{56}, T_{40}, T_{41}...etc.) to the respective $t_{V_1} \rightarrow t_{V_4}$, one can implement any desired SVPWM techinque, including the 12-sector method. For sector 1 of the 12-sector SVPWM (labeled I-12 in 2(a)), the timing diagram is shown in Fig. 3(c). For phase a, the starting logic is "1", and $s_{\mathrm{VSI}}^{\mathrm{a_1}}$ toggles at $(T_0/4+t_{V_1}+t_{V_2})$, $T_0/2$, $2(T_0/4+t_{V_3}+t_{V_4})$. Using of the symmetry per $T_{sw}/2$, the remaining toggling instants are also identified.

V. Evaluation Results

The SVPWM strategy in terms of implementation and harmonics inhibition has been experimentally evaluated by means of the test bench shown in Fig. 4 and with ADT-

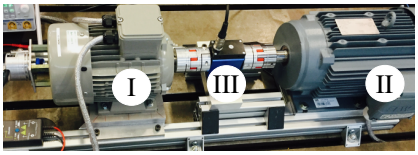

Figure 4: *Test bench: (I) ADT-IPMSM, (II) induction machine and (III) torque sensor.*

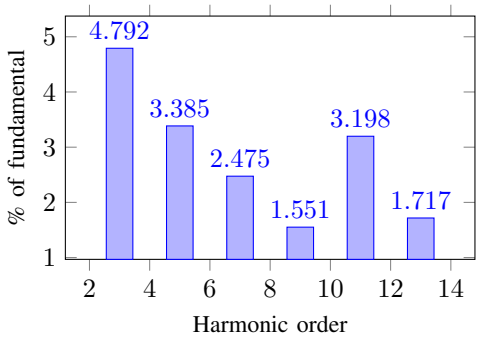

Figure 5: *Harmonic content in the back emf of the ADT-IPMSM.*

Table I: *Parameters of the ADT-IPMSM under study*

Paramter	Value
Stator resistance	$R_\mathrm{s} = 0.8\,\Omega$
Pole-pair	$n_\mathrm{p} = 3$
d-axis inductance	$L_\mathrm{s}^d = 5.5$ mH
q-axis inductance	$L_\mathrm{s}^q = 16.5$ mH
Permanent magnet flux linkage	$\psi_\mathrm{pm} = 174.6$ mWb
Leakage inductance	$L_l = 0.9$ mH
Rated stator current	$i_\mathrm{s,rated} = 4.1$ A
Rated torque	$m_\mathrm{m,rated} = 10.6$ Nm
Rated power	$P_\mathrm{rated} = 4.4$ kW

IPMSM parameters shown in Table I. The two three-phase two level VSIs are switched at a rate of 8 kHz with a dead-time of 1μsec. The control algorithm is implemented on dSPACE DS1007 by means of Matlab/Simulink interface. The PWM signals are sent to the VSIs via the DS5101 PWM card, which is manually flashed and programmed to ensure precise timings and sampling instants. The A/D DS2004 board is triggered by the DS5101 board to carry-out the measurements in the middle of the switching period, ensuring minimum switching noise interference. The field-oriented control has been carried out as in [14], while the xy harmonics were compensated by means of a proportional-resonant (PR) controller, discretized by means of impulse-invariant method [16]. The effectiveness of the proposed switching/timing algorithm and its suitability for different SVPWMs has been evaluated by setting the same reference voltage vector $\boldsymbol{u}_\mathrm{s,ref}^{\alpha\beta}$ (see Fig. 2(a)) in sector I-24 and I-12. Fig. 3 shows that the output of the simulated switching/sampling algorithm matches their equivalent experimental equivalent. Since the 24-sector technique is advantageous in terms of harmonic content, it will be employed in the upcoming results to evaluate the effect of excluding and including the xy subspace regulation.

The induction machine runs as a prime mover rotating at a constant speed of 500 rpm, while the ADT-IPMSM operates in generator mode. The torque command for the ADT-IPMSM was set to the rated torque, corresponding to optimum current reference $\boldsymbol{i}_\mathrm{s,ref}^k = \begin{pmatrix}-2.513, & 5\end{pmatrix}^\top$ A, which were precomputed using the maximum-torque-per-current (MTPC) criteria, as explained in [13]. The harmonic content of the back *emf* is shown in Fig. 5. The presence of 5^th and 7^th harmonics in the back *emf* makes it insufficient to control the $\boldsymbol{i}_\mathrm{s}^{xy}$ by just setting $\boldsymbol{u}_\mathrm{s,ref}^{xy} = 0$. As shown in Fig. 6(a), the presence of $\boldsymbol{i}_\mathrm{s}^{xy}$ leads to a highly distorted stator current (see Fig. 6(b)), even though the fundamental currents are well regulated. Analyzing the stator currents by means of FFT shows substantial 5^th and 7^th harmonic content, resulting in a THD $= 16.32\%$, coinciding with similar practical findings as shown in [10]. Upon considering the effect of compensating the xy current components as in [14], along with proposed SVPWM, significant improvement has been seen in terms of harmonic compensation as evident in Figs. 6(d) and 6(e) as well as enhancing the quality of the harmonic content of the stator currents with THD $= 1.69\%$.

VI. Conclusion

SVPWM techniques for ADTM are well known to synthesize the desired reference voltages, ensuring a high quality output, optimum switching sequence, and minimum switching losses. Applying the different SVPWM methods for ADT-IPMSM as when applying them for ADT-IM would lead to a significant discrepancy in terms of the quality of the stator currents; owing to the non sinusoidal PM flux which compensates, practically, low order harmonics as well as discarding the contribution of the harmonic reference voltages to the calculation of the dwell times. Upon taking this into account, significant improvement was overseen in the quality of the output current as well as nulling the xy currents. Also, the fundamentals for 1N SVPWM was laid which should be reported in the near future. On the other hand, a simple SVPWM digital realization technique has been proposed which is suitable for implementing the different SVPWM methods, as covered in literature. The theoretical findings were corroborated with experimental measurements on a 4.4 kW ADT-IPMSM for the sake of validation.

Acknowledgment

This work is supported by the project AWESCO (H2020-ITN-642682) funded by the European Union's Horizon 2020 research and innovation programme under the Marie Sklodowska-Curie grant agreement No. 642682.

References

[1] I. Gonzalez-Prieto, M. J. Duran, H. S. Che, E. Levi, M. Bermúdez, and F. Barrero, "Fault-tolerant operation of six-phase energy conversion systems with parallel machine-side converters," *IEEE Trans. on Power Electron.*, vol. 31, no. 4, pp. 3068–3079, Apr. 2016.

[2] E. Levi, R. Bojoi, F. Profumo, H. A. Toliyat, and S. Williamson, "Multiphase induction motor drives - a technology status review," *IET Electr. Power Appl.*, vol. 1, no. 4, pp. 489–516, Jul. 2007.

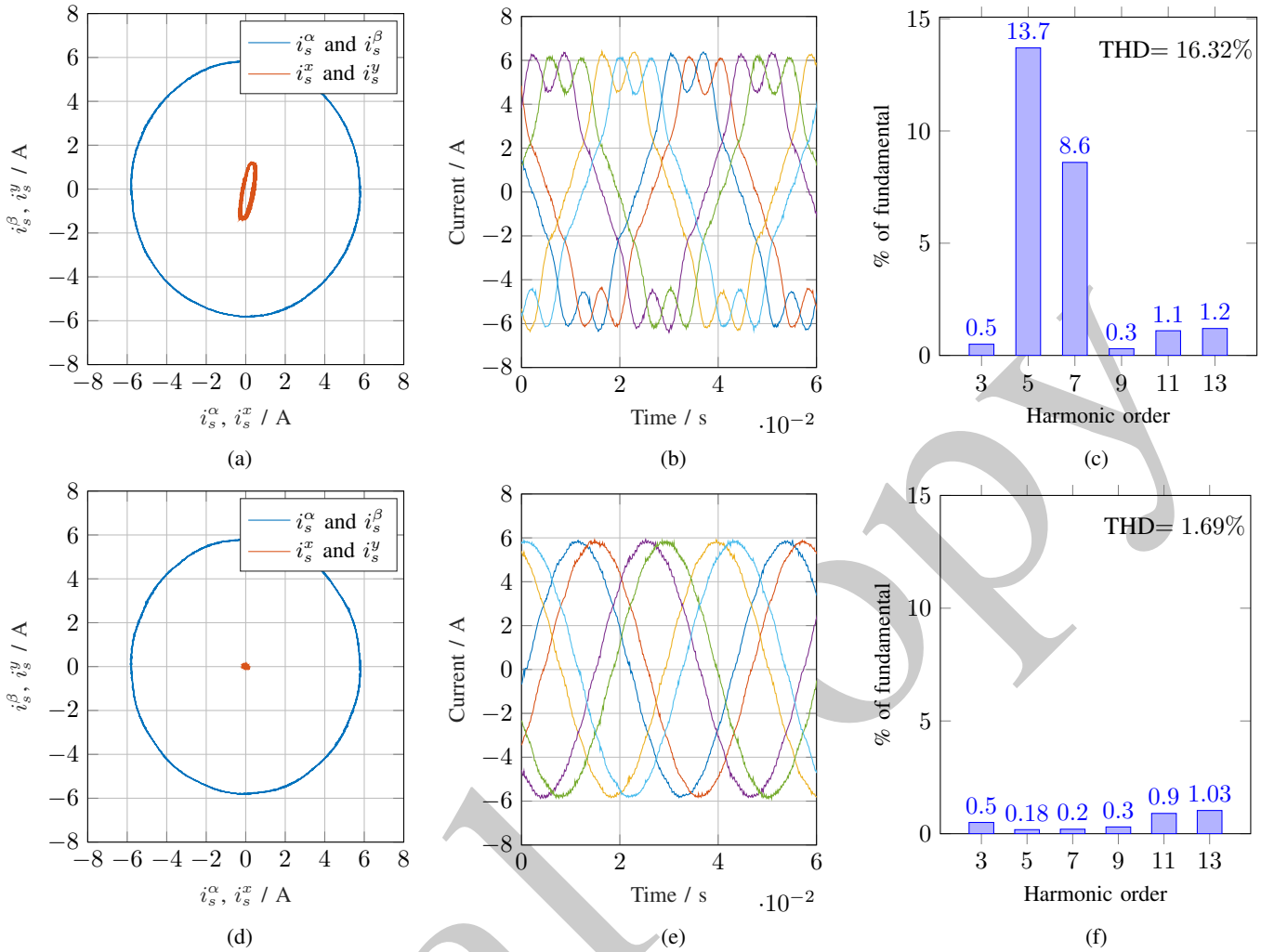

Figure 6: *Effect of discarding and accounting for* $\boldsymbol{u}_{\mathrm{s,ref}}^{xy}$ *within the SVPWM dwell times, top and bottom figures respectively, showing the effect on the {(a),(d)} current loci in the* $\alpha\beta$ *and* xy *planes, {(b),(e)} stator currents, and {(c),(f)} the corresponding FFT for each case.*

[3] D. Hadiouche, H. Razik, and A. Rezzoug, "On the modeling and design of dual-stator windings to minimize circulating harmonic currents for vsi fed ac machines," *IEEE Trans. on Ind. Appl.*, vol. 40, no 2, pp. 506–515, Mar. 2004.

[4] D. Glose and R. Kennel, "Continuous space vector modulation for symmetrical six-phase drives," *IEEE Trans. on Power Electron.*, vol. 31, no 2, pp. 3837–3848, May 2016.

[5] W. N. W. A. Munim, M. Duran, H. S. Che, M. Bermudez, I. Gonzalez-Prieto, and N. A. Rahim, "A unified analysis of the fault tolerance capability in six-phase induction motor drive," *IEEE Trans. on Power Electron.*, vol. 32, no. 10, pp. 7824–7836, Aug. 2016.

[6] D. Hadiouche, L. Baghli, and A. Rezzoug, "Space-vector pwm techniques for dual three-phase ac machine: analysis, performance evaluation, and dsp implementation," *IEEE Trans. on Ind. Appl.*, vol. 42, no. 4, pp. 1112–1122, Jul. 2006.

[7] C. Wang, K. Wang, and X. You, "Research on synchronized svpwm strategies under low switching frequency for six-phase vsi-fed asymmetrical dual stator induction machine," *IEEE Trans. on Ind. Electron.*, vol. 63, no. 11, pp. 6767–6776, Nov. 2016.

[8] K. Marouani, L. Baghli, D. Hadiouche, A. Kheloui, and A. Rezzoug, "A new pwm strategy based on a 24-sector vector space decomposition for a six-phase vsi-fed dual stator induction motor," *IEEE Trans. on Ind. Electron.*, vol. 55, no. 5, pp. 1910–1920, May 2008.

[9] H. S. Che, A. S. Abdel-Khalik, O. Dordevic, and E. Levi, "Parameter estimation of asymmetrical six-phase induction machines using modified standard tests," *IEEE Trans. on Ind. Electron.*, vol. 64, no. 8, pp. 6075–6085, Aug. 2017.

[10] Y. He, Y. Wang, J. Wu, Y. Feng, and J. Liu, "A comparative study of space vector pwm strategy for dual three-phase permanent-magnet synchronous motor drives," in *25th Annual IEEE Appl. Power Electron. Conference and Exposition (APEC)*, pp. 915–919, Feb. 2010.

[11] K. Marouani, L. Baghli, D. Hadiouche, A. Kheloui, and A. Rezzoug, "Discontinuous svpwm techniques for double star induction motor drive control," in *32nd Annual Conference on IEEE Ind. Electron. (IECON)*, pp. 902–907, Nov. 2006.

[12] C. Zhou, G. Yang, and J. Su, "Pwm strategy with minimum harmonic distortion for dual three-phase permanent-magnet synchronous motor drives operating in the overmodulation region," *IEEE Trans. on Power Electron.*, vol. 31, no. 2, pp. 1367–1380, Feb. 2016.

[13] H. Eldeeb, C. M. Hackl, L. Horlbeck, and J. Kullick, "A unified theory for optimal feedforward torque control of anisotropic synchronous machines," *International Journal of Control*, doi:10.1080/00207179.2017.1338359 (early access), pp. 1–30, 2017.

[14] Y. Hu, Z. Q. Zhu, and K. Liu, "Current control for dual three-phase permanent magnet synchronous motors accounting for current unbalance and harmonics," *IEEE Journal of Emerging and Selected Topics in Power Electron.*, vol. 2, no. 2, pp. 272–284, Jun. 2014.

[15] Y. Zhao and T. A. Lipo, "Space vector pwm control of dual three-phase induction machine using vector space decomposition," *IEEE Trans. on Ind. Appl.*, vol. 31, no. 5, pp. 1100–1109, Sep. 1995.

[16] H. Eldeeb, A. Massoud, A. S. Abdel-Khalik, and S. Ahmed, "A sensorless kalman filter-based active damping technique for grid-tied vsi with lcl filter," *International Journal of Electrical Power & Energy Systems*, vol. 93, pp. 146–155, Jun. 2017.